APPLIED ORGANOMETALLIC CHEMISTRY
Appl. Organometal. Chem. 2001; **15**: 178–196

Various ligand-stabilized metal nanoclusters as homogeneous and heterogeneous catalysts in the liquid phase

Naoki Toshima,[1]* Yukihide Shiraishi,[1] Toshiharu Teranishi,[2] Mikio Miyake,[2] Toshihiro Tominaga,[3] Hiroshi Watanabe,[3] Werner Brijoux,[4] Helmut Bönnemann[4] and Günter Schmid[5]

[1]Department of Materials Science and Engineering, Science University of Tokyo in Yamaguchi, Onoda-shi, Yamaguchi 756-0884, Japan
[2]School of Materials Science, Japan Advanced Institute of Science and Technology, 1-1 Asahidai, Tatsunokuchi, Nomi, Ishikawa 923-1292, Japan
[3]Department of Applied Chemistry, Faculty of Engineering, Okayama University of Science, Ridai-cho, Okayama 700-0005, Japan
[4]Max-Planck-Institut für Kohlenforschung, Kaiser-Wilhelm-Platz 1, D-45466 Mülheim an der Ruhr, Germany
[5]Universität GH Essen, FB8 Anorganische Chemie, Universitätsstrasse 5-7, D-45117 Essen, Germany

Ligand-stabilized noble metal nanoclusters, prepared by various chemical methods by different research groups in Japan and Germany, were characterized and examined by a common method for application to the catalysis for hydrogenation of olefins in homogeneous and heterogeneous systems in the liquid phase. The mean diameters of palladium, platinum, rhodium and Pd/Pt nanoclusters stabilized by various ligands range from 1.3 to 3.2 nm if prepared by a single reaction, and from 2.2 to 4.0 nm if prepared by a stepwise growth method. The Stokes radii of metal nanoclusters stabilized by surfactants range from 1.7 to 2.1 nm, suggesting a thickness of the protective layer from 1.1 to 1.4 nm, whereas those stabilized by polymers give much larger values, suggesting the formation of aggregates. The catalytic activities of the metal nanoclusters, evaluated by hydrogenation of 1,3-cyclooctadiene and methyl acrylate, depend mainly upon the particle size, i.e. the smaller the size, the higher the activity. However, a strongly interacting ligand like tetraoctylammonium halide and 1,10-phenanthroline can disturb the hydrogenation. In contrast, the activities of heterogeneous catalysts supported on charcoal depend strongly on the covering strength of the stabilizer.

Keywords: metal cluster; nanoparticle; nanocluster; colloidal dispersion; poly(*N*-vinyl-2-pyrrolidone); 3-(dimethyldodecylammonio)propanesulfonate; 1,10-phenanthroline; tetraoctylammonium bromide; ligand; TEM; HRTEM; diffusion coefficient; hydrogenation catalyst; supported catalyst; Taylor dispersion method

Received 11 July 2000; accepted 7 November 2000

INTRODUCTION

Recently, much attention has been paid to nanoparticles as a building block of nanostructures and/or nanotechnology.[1] The terminology of 'nanoparticle' could be based on the technological background. The term 'cluster' is used for an aggregate of molecules or atoms with a precise structure. In the case of metal particles, 'metal cluster' often means the aggregate of metal atoms that contains less than about ten metallic atoms, for example $[Ni_5(CO)_{12}]^{2-}$. They are the subject for the usual organometallic chemistry. Recently, however, metal clusters, that contain larger numbers of metal atoms than the conventional one, have attracted scientists' attention. For example, Au_{55} has a size of 1.4 nm in diameter. Some people use the terminol-

* Correspondence to: Naoki Toshima, Department of Materials Science and Engineering, Science University of Tokyo in Yamaguchi, Onoda-shi, Yamaguchi 756-0884, Japan.
Contract/grant sponsor: Japan Society for the Promotion of Science (JSPS).
Contract/grant sponsor: Deutsche Forschungsgemeinschaft (DFG).

ogy of 'giant metal cluster' for these clusters in order to distinguish it from the conventional low nuclearity organometallic clusters. In this paper, we prefer to use the terminology 'metal nanocluster', which means a metal cluster of nanometer scale.

Metal nanoclusters cannot be stabilized without stabilizers, which are usually organic ligands or polymers, and more or less coordinate to metal nanoclusters.[2] These stabilized noble-metal nanoclusters are of great interest for catalytic applications, e.g. hydrogenation of double bonds.[3,4] Many research groups are working on the preparation of noble metal nanoclusters and their application to catalysis.[5] However, each research group has prepared similar metal nanoclusters by their own preparation method, and applied them to different reactions. So, people in general cannot understand which metal nanocluster and which preparation method is the best among those proposed.

From this background, the present authors, from different research groups, started a joint research project supported by the Japan Society for the Promotion of Science and Deutsche Forschungsgemeinschaft. In this project, individual members have prepared noble metal nanoclusters by their own favorite method. Then, all the nanocluster samples were characterized by the same method by a single person among the members, and applied to the same reaction under the same reaction conditions being measured by a single person among the members. In this way we believe that a complete comparison can be carried out among the different types of nanocluster. The results are very interesting. Not only the cluster size, but also the stabilizing ligand can have a large effect on the catalytic activities.

EXPERIMENTAL

Preparation of noble-metal nanoclusters

Simultaneous alcohol-reduction method

$$PdCl_2 + C_2H_5OH \longrightarrow Pd_{nanocluster} + CH_3CHO + 2\,HCl$$

$$H_2PtCl_6 + 2\,C_2H_5OH \longrightarrow Pt_{nanocluster} + 2\,CH_3CHO + 6\,HCl$$

$$RhCl_3 + 1.5\,C_2H_5OH \longrightarrow Rh_{nanocluster} + 1.5\,CH_3CHO + 3\,HCl$$

The group of Yamaguchi used an alcohol reduction method to prepare noble-metal nanoclusters in the presence of poly(*N*-vinyl-2-pyrrolidone) (PVP).[6] The colloidal dispersions of the Pd/Pt (4/1) bimetallic nanoclusters protected by PVP were prepared in the following way. Solutions of hexachloroplatinic(IV) acid (0.13 mmol in 500 ml of water) were prepared by dissolving the corresponding crystalline material in water. Ethanol solutions of palladium(II) chloride (0.53 mmol in 500 ml of ethanol) were prepared by stirring dispersions of $PdCl_2$ powder in ethanol. An ethanol/water (1/1, v/v) solution, containing two kinds of metal ion and PVP (K-30, 73.4 mg, MW 40 000, 0.66 mmol as a monomeric unit) as a protecting polymer, was refluxed at about 90–95 °C for 3 h under nitrogen. The amount of PVP used for the present preparation is much smaller than that used in the previous reports,[6] because a lesser amount of stabilizer was preferred for the preparation of supported catalysts. The colloidal dispersion of Pd/Pt bimetallic nanoclusters, thus prepared (abbreviated as Pd/Pt–PVP), have a brownish-black color and are sufficiently stable.

The colloidal dispersions of the palladium and platinum monometallic nanoclusters (Pd–PVP–Et(1/1) and Pt–PVP respectively) were prepared by a similar method in an ethanol/water (1/1, v/v) solution. Those of rhodium monometallic nanoclusters (Rh–PVP) were prepared in ethanol. The total amount of metals was always kept as 0.66 mmol in 1 l of the mixed solution.

Stepwise alcohol-reduction method

$$H_2PdCl_4 + C_2H_5OH \longrightarrow Pd_{nanocluster} + CH_3CHO + 4\,HCl$$

The group of Ishikawa used a stepwise alcohol-reduction method to prepare palladium nanoclusters with different size.[7] A 2.0 mM H_2PdCl_4 aqueous solution was prepared by mixing $PdCl_2$ (106.4 mg, 0.6 mmol), 0.2 M HCl solution (6.0 ml) and distilled water (294 ml). The mixtures of the 2.0 mM H_2PdCl_4 aqueous solution (80 ml, 0.16 mmol of Pd), water (400 ml), 1-propanol (320 ml) and PVP (711 mg, 6.4 mmol as a monomeric unit) were refluxed in a 1 l flask for 3 h in air to synthesize the PVP-stabilized palladium nanoclusters (abbreviated as Pd–PVP–Pr (2/3)).

In order to produce larger palladium nanoclusters, mixtures of 2.0 mM H_2PdCl_4 aqueous solution (80 ml), water (560 ml), ethanol (160 ml) and PVP (178 mg, 1.6 mmol as a monomeric unit)

were refluxed under similar conditions (Pd–PVP–Et(1/4)). Such a one-step synthesis is adequate to obtain palladium nanoclusters of 1.0 –3.0 nm, whereas it is quite difficult to synthesize palladium nanoclusters larger than 3.0 nm. So, the monodispersed PVP-stabilized palladium nanoclusters, synthesized in a one-step reaction, were used as seeds for stepwise growth to obtain nanoclusters larger than 3.0 nm without significant change in size distribution. The Pd–PVP–Et(1/4) nanoclusters, having a mean diameter of 2.53 nm with narrow size distribution ($\sigma = 0.400$ nm), were employed as starting seeds for stepwise growth. The second growth of PVP-stabilized palladium nanoclusters was carried out by mixing 0.2 mM colloidal dispersion of Pd–PVP–Et(1/4) (400 ml) with 0.2 mM H_2PdCl_4 in an ethanol/water (1/4, v/v) solution (400 ml), followed by refluxing the mixture for 3 h (Pd–PVP–Et(1/4)2). The third growth was conducted in a similar manner (Pd–PVP–Et(1/4)3). The synthesized samples were precipitated by addition of a large amount of diethyl ether, followed by filtering, drying under vacuum at 80 °C, and then crushing them in a mortar and pestle.

The concentrations of palladium in a series of PVP-stabilized palladium nanoclusters were determined by elemental analysis. From elemental analysis, the palladium contents were estimated to be 3.43 wt%, 12.1 wt%, 22.2 wt%, and 42.0 wt% for Pd–PVP–Pr(2/3), Pd–PVP–Et(1/4), Pd–PVP–Et(1/4)2, and Pd–PVP–Et(1/4)3 respectively.

Triorganoborate-reduction method

The group of Mülheim used triethylhydroborate, BEt_3H, as a reductant for preparation of palladium, platinum and rhodium nanoclusters stabilized by surfactants like 3-(dimethyldodecylammonio)propanesulfonate (DDAPS) and tetraoctylammonium chloride (TOAC) or bromide (TOAB).[8]

Pd–DDAPS:

$$PdCl_2 + 2\,[(C_{12}H_{25})(CH_3)_2N{-}(CH_2)_3{-}SO_3Li]^+ [BEt_3H]^- \xrightarrow{THF} Pd_{nanocluster} + 2\,[(C_{12}H_{25})(CH_3)_2 N^+{-}(CH_2)_3{-}SO_3^-] + 2\,LiCl + 2\,BEt_3 + H_2\uparrow$$

A suspension of $PdCl_2$ (0.177 g, 1 mmol) and DDAPS (0.67 g, 2 mmol) in THF was reduced by adding dropwise a solution of 1.56 M $LiBEt_3H$ in THF (0.9 ml, 1.4 mmol) over 16 h at room temperature (rt). After adding 2 ml of absolute acetone, the reaction mixture was stirred for 1 h. The suspension of the gray–brown powders in THF was allowed to settle over several hours. The supernatant solution was removed and, after drying the gray powder in vacuum (0.1 Pa) at rt, the water-soluble palladium nanoclusters were isolated.

Pd–TOAC:

$$PdCl_2 + 2\,N(C_8H_{17})_4BEt_3H \xrightarrow{THF} Pd_{nanocluster} + 2\,N(C_8H_{17})_4Cl + 2\,BEt_3 + H_2\uparrow$$

A 0.258 M $N(C_8H_{17})_4BEt_3H$ in THF (36 mL) was added within 16 h at rt to a vigorously stirred suspension of $PdCl_2$ (0.830 g, 4.7 mmol) in THF (150 ml). To the resulting black–brown palladium-organosol, 5 ml of acetone were added and the solution was stirred for 30 min to quench an excess reductant. This organosol was either supported directly on a carrier or worked up to increase the metal content of the ligand-stabilized nanoclusters.

For the work-up the volatile compounds were removed in vacuum at rt and dried in vacuum (0.1 Pa) for 16 h. Then the waxy red–black residue was dissolved in 10 ml of diethyl ether and stirred in air for 2 h. Addition of 100 ml of ethanol caused the formation of a grayish precipitate. The precipitate was allowed to settle down for several hours before the supernatant solution was removed with a pipette. Drying in vacuo (0.1 Pa, rt, 16 h) yielded a black waxy powder with a metal content of 32 wt% palladium, proved to be redispersible in THF.

Pt–DDAPS:

$$PtCl_2 + 2\,[(C_{12}H_{25})(CH_3)_2N{-}(CH_2)_3{-}SO_3Li]^+ [BEt_3H]^- \xrightarrow{THF} Pt_{nanocluster} + 2\,[(C_{12}H_{25})(CH_3)_2 N^+{-}(CH_2)_3{-}SO_3]^- + 2\,LiCl + 2\,BEt_3 + H_2\uparrow$$

A suspension of DDAPS (14.0 g, 41.7 mmol) in THF (300 ml) was treated by ultrasonic irradiation for 10 min and a solution of $LiBEt_3H$ (4.38 g, 41.35 mmol) in THF (19 ml) was added dropwise under stirring at 20 °C. The resulting clear solution was added to a suspension of $PtCl_2$ (5.5 g, 20.67 mmol) in THF (300 ml) at rt in 24 h. The resulting black reaction mixtures were stirred for a further 10 h at rt. Then 10 ml of acetone was added. The precipitate was allowed to settle for 1 h before the clear supernatant solution was removed by applying pressure using inert gas on the liquid surface. This procedure was repeated and the black–brown residue was dried at rt and 0.1 Pa for 1 h. The product (17.0 g) proved soluble in water and ethanol, but insoluble in acetonitrile (cold), THF, toluene, ether, acetone, and pentane. Thereafter, the residue was dissolved in 45 ml of

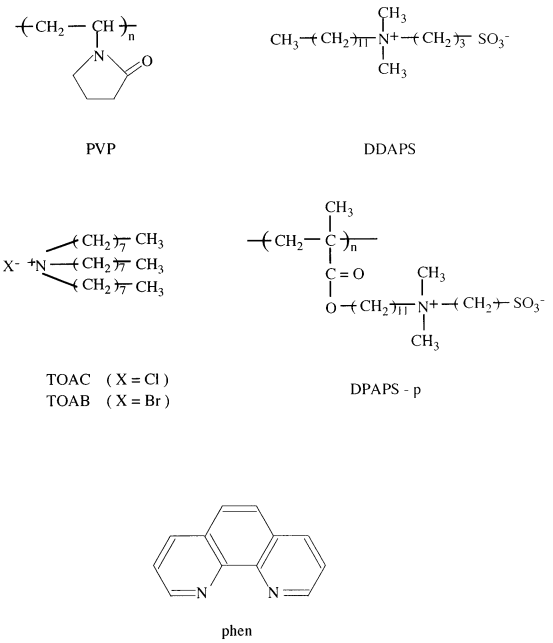

Figure 1 Chemical structures of the stabilizers used in the present study.

water by treating with ultrasound and then addition of 110 ml of acetonitrile to the solution caused the formation of a dark grayish-brown precipitate. The precipitate was allowed to settle for 16 h and a clear supernatant solution was removed by applying pressure using inert gas on the liquid surface. Drying in vacuum (0.1 Pa, rt, 3 h) yielded a gray colloidal powder (5.3 g), which proved to be very soluble in water and ethanol. Metal content: 61.6 wt% platinum.

Pt–(DDAPS)p: 0.25 mmol of $H_2PtCl_6{\cdot}6H_2O$ and the polysoap DDAPS-p (0.5 mmol, see Fig. 1 for the chemical structure) were dissolved or suspended in 15 ml of water and a solution of $LiBH_4$ (1.5 mmol) was added dropwise at a slow speed to prevent foaming. After 60 min at 20 °C a clear brownish-black solution resulted, and water was removed by freeze drying. The polysoap-stabilized platinum nanoclusters were obtained as black solids, which were stable against atmospheric oxygen. They were hygroscopic and contained 9.15 wt% platinum.

Pt–TOAB:

$$PtBr_4 + 4\,N(C_8H_{17})_4BEt_3H \rightarrow Pt_{nanocluster} + 4\,N(C_8H_{17})_4Br + 4\,BEt_3 + 2\,H_2\uparrow$$

Under argon a solution of $N(C_8H_{17})_4[BEt_3H]$ in THF (211 ml, 0.19 M) was added within 16 h at 20 °C to a stirred solution of anhydrous $PtBr_4$ (5.15 g, 10 mmol) in THF (650 ml). The clear, dark black–brown solution was concentrated in vacuo, and the resulting black–brown, waxy residue was dried for 16 h at rt at 0.1 Pa. The product (23.4 g), consisting of 8.1 wt% platinum, is soluble in THF, ether, toluene and acetone, but insoluble in ethanol. The residue was suspended in 20 ml of technical quality ether in air. Addition of 400 ml of technical quality ethanol induced the formation of a gray–black precipitate. The suspension was allowed to stand for 16 h, before removing the clear supernatant solution by argon pressure on the liquid surface. After drying in vacuum (0.1 Pa, 16 h, rt) a gray platinum nanocluster powder (3.1 g) consisting of 61.2 wt% platinum was isolated, which is very soluble in THF.

Rh–DDAPS:

$$RhCl_3 + 3\,[(C_{12}H_{25})(CH_3)_2N{-}(CH_2)_3{-}SO_3Li]^+ [BEt_3H]^- \xrightarrow{THF} Rh_{nanocluster} + 3\,[(C_{12}H_{25})(CH_3)_2 N{-}(CH_2)_3{-}SO_3]^- + 3\,LiCl + 3\,BEt_3 + 1.5\,H_2$$

A suspension of DDAPS (9.86 g, 29.4 mmol) in THF (300 ml) was treated for 10 min by ultrasonic irradiation and a solution of $LiBEt_3H$ (3.25 g, 30.78 mmol) in THF (19 ml) was added dropwise under stirring at 20 °C. The resulting clear solution was added to a suspension of $RhCl_3$ (2.05 g, 9.7 mmol) in THF (300 ml) at 65 °C in 28 h. The resulting black reaction mixture was stirred for a further 2 h at 65 °C and, after cooling at 20 °C, 10 ml of acetone was added. The precipitate was allowed to settle for 16 h before the clear supernatant solution was removed by applying pressure using inert gas on the liquid surface. This procedure was repeated and the black–brown residue was dried at 20 °C and 0.1 Pa for 1 h. The product (11.21 g) proved soluble in water and ethanol, but insoluble in acetonitrile (cold), THF, toluene, ether, acetone, and pentane, and contained 7.09 wt% rhodium. Thereafter, the residue was dissolved in 14 ml of water and addition of 30 ml of acetonitrile caused the formation of a dark grayish–brown precipitate. The precipitate was allowed to settle for 16 h and the solution was heated to 80 °C for 10 min before the clear supernatant solution was removed by applying pressure using inert gas on the liquid surface. Drying in vacuum (0.1 Pa, 20 °C, 3 h) yielded a gray nanocluster powder (3.98 g),

which proved to be very soluble in water and ethanol. Metal content: 25.21 wt% rhodium.

Rh–TOAB:

$$RhCl_3 + 3\,N(C_8H_{17})4\,BEt_3H \longrightarrow Rh_{nanocluster} + 3\,N(C_8H_{17})4\,Br + 3\,BEt_3 + 1.5H_2$$

A solution of $RhCl_3{\cdot}3H_2O$ (2.369 g, 8.997 mmol) and $N(C_8H_{17})_4Br$ (14.72 g, 26.92 mmol) in THF (150 ml) was evaporated three times in vacuum to remove the water (infrared-control). 4.741 g (2.563 mmol) of the dark-red dried $Rh[N(C_8H_{17})_4]_2Br_2Cl_3$ were dissolved in 600 ml of THF. A solution of 4.351 g (7.689 mmol) $N(C_8H_{17})_4BEt_3H$ in 100 ml of THF was added dropwise to this solution at 55 °C in 24 h. The black–brown colloidal dispersion was stirred at rt for 16 h. Acetone (5 ml) was added and the reaction mixture was stirred for 2 h. The solvent was evaporated at 40 °C and the nanoclusters were dried at 40 °C and 0.1 Pa for 16 h, yielding 8.32 g of black–brown rhodium nanoclusters, which are very soluble in THF, toluene and acetone.

3-Methylbutanol-reduction method

$$Pd(OCOCH_3)_2 + (CH_3)_2CH{-}CH_2{-}CH_2{-}OH \xrightarrow{phen} Pd_{nanocluster} + (CH_3)_2CHCH_2CHO + 2\,CH_3COOH$$

The group of Essen used 3-methylbutanol as a reductant and 1,10-phenanthroline (phen) as a stabilizer to synthesize palladium nanoclusters.[9] Palladium acetate (300 mg, 1.29 mmol) and 1,10-phenanthroline (29 mg, 0.16 mmol) were dissolved in 3-methylbutanol (80 ml) and heated to 60 °C under nitrogen with stirring. After 3 days a fourfold amount of petroleum ether was added and the black suspension centrifuged for 30 min at 5000 rpm. The colorless solution was separated and the black solid dried under vacuum. The yield was quantitative. Elemental analyses showed the structure of palladium nanoclusters as $[Pd_6(O)(phen)_2]_n$.

Preparation of supported palladium catalysts

2 to 4 g of activated carbon (PCT/EP92/0070 to H. Bönnemann, W. Brijoux, R. Brinkmann, E. Dinjus, R. Fretzen, and B. Korall, Studiengesellschaft Kohle GmbH.) were suspended in about 50 ml of absolute THF, and an appropriate amount of the palladium colloid, dissolved or suspended in THF, was added thereto. The mixture was stirred overnight, followed by filtration over a D4-frit from the absolutely colorless metal-free solution. The activated carbon covered with the palladium colloid was dried for 16 h at rt under high vacuum (0.1 Pa), whereafter about 10% of the solvent remained absorbed. Thus, the palladium contents can be adjusted to about 5%.

Measurement of the size of nanoclusters

The metal nanoclusters employed here were characterized by Dr Teranishi at Ishikawa by transmission electron microscopy (TEM) at 125 kV on an Hitachi H-7100 electron microscope and high-resolution TEM (HRTEM) at 300 kV on an Hitachi H-9000 NAR. Samples for TEM were prepared by placing a drop of the colloidal dispersion of metal nanoclusters onto a carbon-coated copper grid, followed by naturally evaporating the solvent. The mean diameter and standard deviation were calculated by counting 200 particles with a magnifying glass from the TEM image at 400 000 ×magnification. The crystallinity of the metal nanoclusters was observed by high resolution TEM (HRTEM).

Measurement of diffusion coefficients

The diffusion coefficients were measured and calculated at Okayama using a Taylor dispersion method.[10,11] In this method, a small amount of solution is injected into a solvent flowing through a capillary tube. As a result of a combination of molecular diffusion and convection, the solute is dispersed along the tube. By suitable choices of experimental conditions the height E of the dispersion peak at the detection point at time t can be expressed by

$$E(t) = (t_R/t)^{1/2} E_{max}[\exp\{-12D(t - t_R)^2/r^2 t\}] \quad (1)$$

where t_R is the residence time, r is the capillary radius, and D is the diffusion coefficient. A Teflon tube was used as a capillary; this was 0.5 mm in inner diameter, 20 m in length, coiled in a 35 cm circle, and was placed in a water bath thermostatically controlled at 25.00 ± 0.02 °C. Solute concentrations were detected by a spectrophotometric detector (Waters 490) at a wavelength of 400 or 500 nm. Output signals from the detector were transferred to a personal computer and were

analyzed using data analysis software (Origin, Microcal Software, Inc.). Other details have been described elsewhere.[12]

Hydrogenation in homogeneous systems

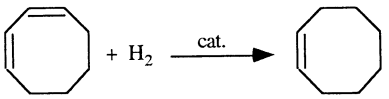

$$CH_2 = CHCOOCH_3 + H_2 \xrightarrow{\text{cat.}} CH_3\text{-}CH_2\text{-}COOCH_3$$

The catalytic activities of the given metal nanoclusters in a homogeneous system were measured by Dr Shiraishi of Yamaguchi for the hydrogenation of 1,3-cyclooctadiene (COD) and methyl acrylate (MA) in the following way.

The ethanol dispersions of metal nanoclusters (0.3 ml, 2.0×10^{-4} mmol of metal) and 18.7 ml of ethanol were added into a flask, the atmosphere of which was previously replaced with hydrogen at atmospheric pressure. The mixtures were stirred for 2 h at 30 °C to activate the catalyst. Then, to these mixtures, an ethanol solution (1 ml) containing 0.5 mmol of either 1,3-cyclooctadiene or methyl acrylate was added, keeping the total pressure at 1 atm. The progress of hydrogenation was followed by a hydrogen uptake under atmospheric pressure.

Hydrogenation in a heterogeneous system (cinnamic acid test)

$$C_6H_5\text{—}CH\text{═}CH\text{—}COOH + H_2 \longrightarrow C_6H_5\text{—}CH_2\text{—}CH_2\text{—}COOH$$

The palladium catalyst 10.2226 g was weighed into a 100 ml dropping funnel. The dropping funnel was placed onto the reactor and the complete apparatus was evacuated several times and refilled with hydrogen. The catalyst in the dropping funnel was subsequently suspended in 20 ml of ethanol (equilibrated at 25 °C) and transferred into the reactor. A solution (80 ml) of cinnamic acid (125 g, 0.84 mol) per liter of ethanol (also equilibrated at 25 °C) was then pipetted into the funnel and dropped into the reactor. Afterwards the funnel was rinsed with 20 ml of ethanol. The catalyst suspension was equilibrated with hydrogen at 25.0 ± 0.2 °C. While the reactor was being charged, it was constantly being flushed with hydrogen. The self-aspirating hollow stirrer was not yet in use. After the pressure equilibrated, the line to the 1 l precision gas burette (mercury-sealed, coupled to a recorder) was opened and the catalyst suspension was stirred with a speed of 2000 rpm. The hydrogen consumption was registered over a period of 6 min, whereby the first minute was not utilized in the evaluation. Between the second and sixth minutes, a hydrogen consumption of 347.0 ml was measured for Pd–DDAPS on C catalyst (run 1), for example. Conversion to normal conditions gives a consumption of 1.063 ml s^{-1}. From this, after considering a 10% content of solvent in the catalyst, an activity of 0.506 mol-H_2 mol-Pd^{-1} s^{-1} (= 30.36 mol-H_2 mol-Pd^{-1} min^{-1}) can be calculated.

RESULTS AND DISCUSSION

Preparation of various ligand-stabilized metal nanoclusters

Various ligand-stabilized noble-metal nanoclusters were prepared by chemical methods from the corresponding metal ions at different research groups in Japan and Germany. Alcohols were used as a reductant by the groups of Yamaguchi and Ishikawa. The Yamaguchi group used a one-step simultaneous reduction method, whereas the Ishikawa group used a stepwise reduction method to prepare the nanoclusters with rather large sizes. The group at Mülhelm a. d. Ruhr used lithium trialkylhydroborates as a reductant, whereas the group at Essen used 3-methylbutanol in the present case. All the metal nanoclusters used in the present paper are summarized in Table 1 with the abbreviations. The chemical structures of the stabilizers used here are illustrated in Fig. 1.

TEM observation of various metal nanoclusters

Figure 2 shows the TEM photographs and size distributions of Pd–PVP–Et(1/1), Pt–PVP, Rh–PVP, and Pd/Pt–PVP nanoclusters. These nanoclusters have similar sizes with mean diameters 2.5–3.0 nm and contain the five-shell clusters as a main product. However, the size distributions of the Pd–PVP–Et(1/1) and Pt–PVP nanoclusters are slightly wide ($\sigma > 0.50$ nm), compared with the Rh–PVP and Pd/Pt–PVP nanoclusters ($\sigma < 0.40$ nm). Aggregation is observed for Rh–PVP nanoclusters, as shown in Fig. 2c.

TEM photographs and size distributions of Pt–(DDAPS)p, Pt–DDAPS, Rh–DDAPS, and Pd–DDAPS are presented in Fig. 3. The Pt–(DDAPS)p

Table 1 Preparation and abbreviation of noble-metal nanoclusters

Abbreviation	Stabilizer (R)[a]	Reductant	Preparation site
Pd–PVP–Et(1/1)	PVP (1)	EtOH/H_2O (1/1)	Yamaguchi
Pd–DDAPS	DDAPS (2)	$LiBEt_3H$	Mülheim
Pd–phen	phen (0.12)	3-Methylbutanol	Essen
Pd–PVP–Pr(2/3)	PVP (40)	1-PrOH/H_2O (2/3)	Ishikawa
Pd–PVP–Et(1/4)	PVP (10)	EtOH/H_2O (1/4)	Ishikawa
Pd–PVP–Et(1/4)2	PVP (5)	EtOH/H_2O (1/4)	Ishikawa
Pd–PVP–Et(1/4)3	PVP (2.5)	EtOH/H_2O (1/4)	Ishikawa
Pd–TOAC	TOAC (2)	BEt_3H^-	Mülheim
Pd/Pt–PVP	PVP (1)	EtOH/H_2O	Yamaguchi
Pt–PVP	PVP (1)	EtOH/H_2O (1/1)	Yamaguchi
Pt–DDAPS	DDAPS (2)	$LiBEt_3H$	Mülheim
Pt–(DDAPS)p	DDAPS-p (2)	$LiBEt_3H$	Mülheim
Pt–TOAB	TOAB (4)	BEt_3H^-	Mülheim
Rh–PVP	PVP (1)	EtOH/H_2O (1/1)	Yamaguchi
Rh–DDAPS	DDAPS (3)	$LiBEt_3H$	Mülheim
Rh–TOAB	TOAB (3)	BEt_3H^-	Mülheim

[a] R: mole ratio of monomeric unit of polymer to metal.

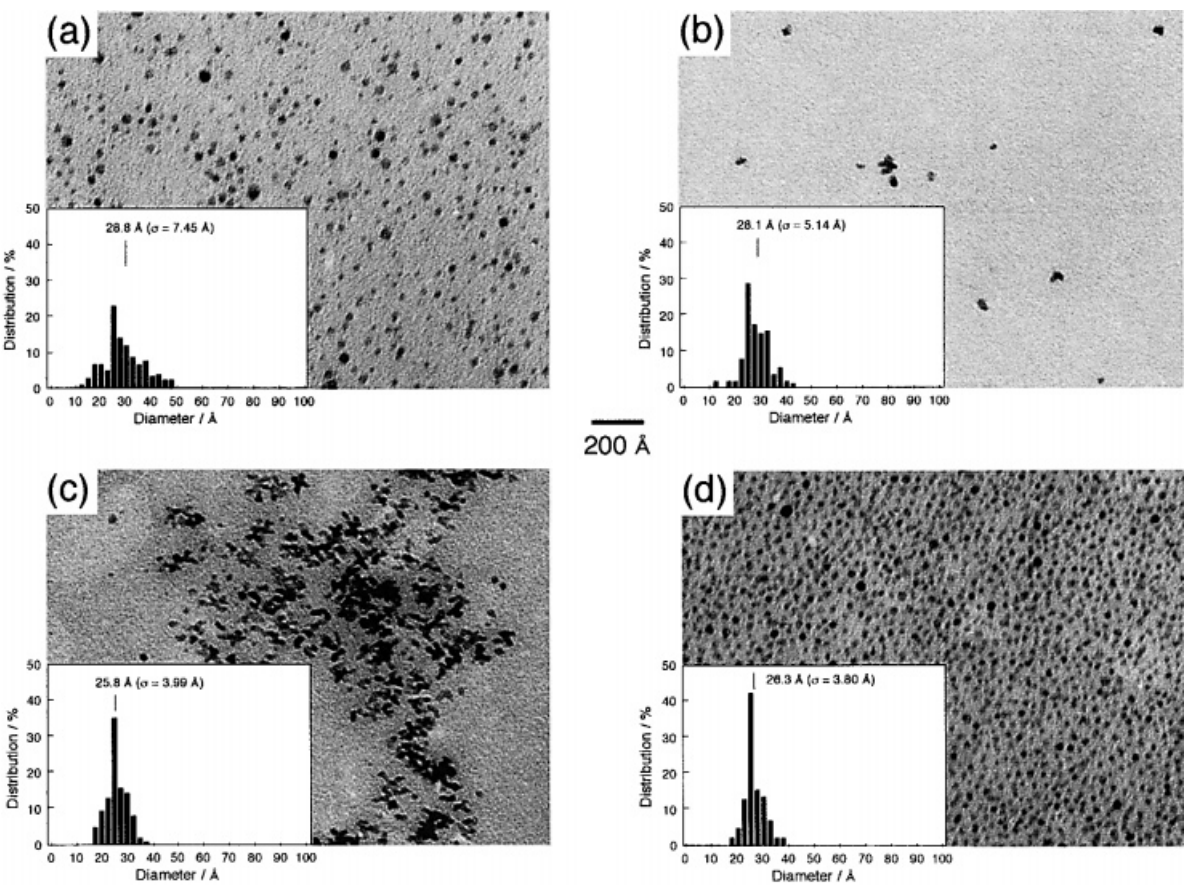

Figure 2 TEM photographs of (a) Pd–PVP–Et(1/1), (b)Pt–PVP, (c)Rh–PVP, and (d) Pd/Pt–PVP nanoclusters and size distributions estimated from the photographs.

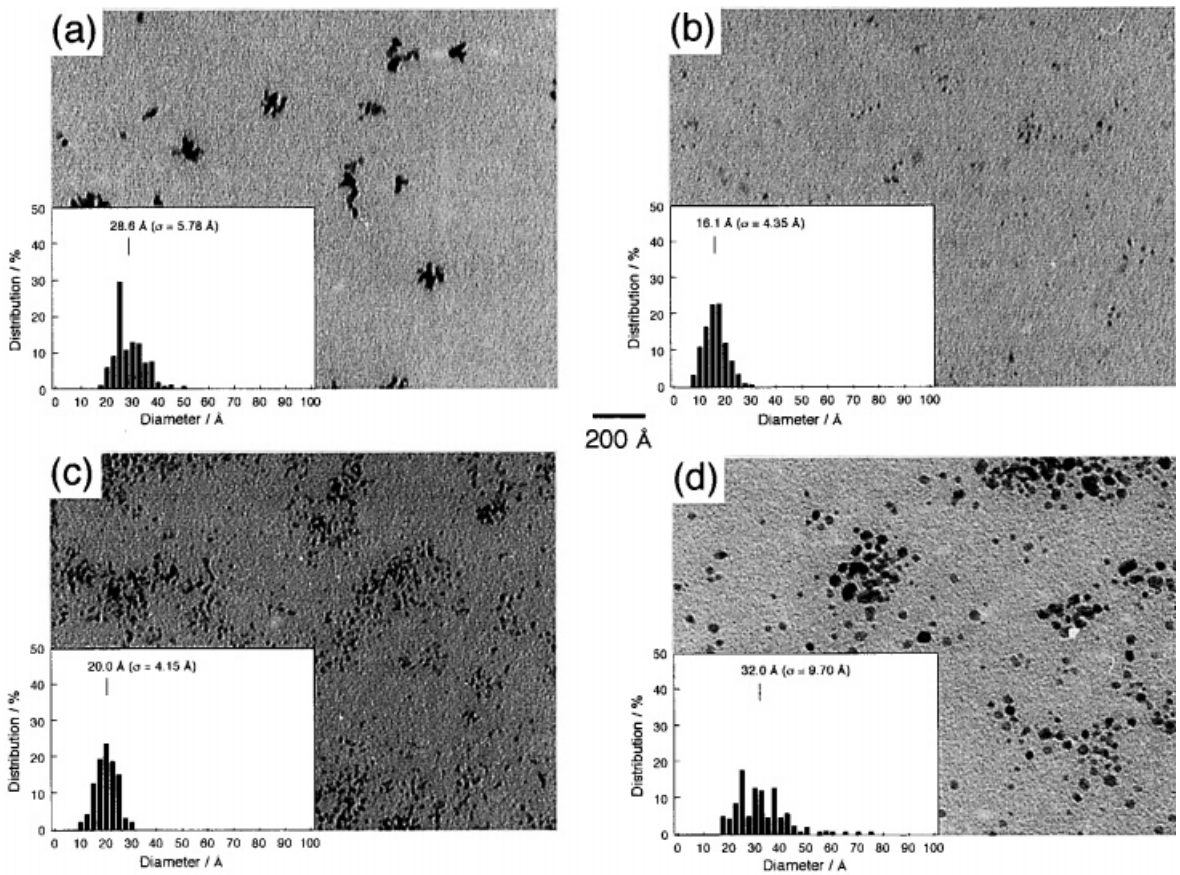

Figure 3 TEM photographs of (a) Pt–(DDAPS)p, (b) Pt–DDAPS, (c) Rh–DDAPS, and (d) Pd–DDAPS nanoclusters and size distributions estimated from the photographs.

nanoclusters have both a mean diameter and a size distribution similar to Pt–PVP, and show aggregations of *ca* 15.0 nm in size. On the other hand, the Pt–DDAPS nanoclusters are observed as small and isolated particles of 1.61 nm in mean diameter with a narrow size distribution. The Rh–DDAPS nanoclusters of 2.0 nm show monodispersity, but severe aggregation occurs as observed in Rh–PVP nanoclusters. The size distribution of Pd–DDAPS nanoclusters is the widest of all the nanoclusters employed in this research.

The palladium nanoclusters stabilized by 1,10-phenanthroline (phen) and oxygen are 2.63 nm in size with a slightly wide distribution, as shown in Fig. 4.

The TEM photographs and size distributions of Pd–PVP–Pr(2/3), Pd–PVP–Et(1/4), Pd–PVP–Et (1/4)2, and Pd–PVP–Et(1/4)3 are shown in Fig. 5. The Pd–PVP–Pr(2/3) and Pd–PVP–Et(1/4) nanoclusters have mean diameters of 2.19 nm (σ = 0.493 nm) and 2.53 nm (σ = 0.400 nm) respectively (Fig. 5a and 5b). The generation of Pd–PVP–Pr(2/3) with a smaller size than Pd–PVP–Et(1/1) was achieved both by the use of a larger amount of protective polymer (PVP), and by a faster reduction of $[PdCl_4]^{2-}$ to Pd^0 with 1-propanol, resulting in the formation of a larger number of nuclei. The Pd–PVP–Et(1/4)2 and Pd–PVP–Et(1/4)3 nanoclusters were obtained by the stepwise reaction starting from Pd–PVP–Et(1/4). As shown in Fig. 5c and d, the nanoclusters are clearly growing with increasing number of reaction steps, indicating that the nanoclusters in the solution serve as nuclei for larger ones. The diameter d of nanoclusters obtained by a stepwise reaction can be calculated using Eqn [2]:[12]

$$d = d_0 \sqrt[3]{\frac{n_i + n_m}{n_m}} \qquad (2)$$

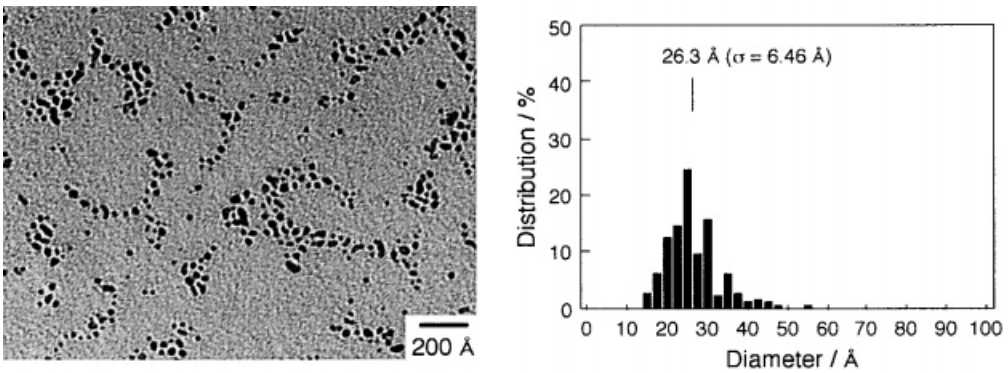

Figure 4 TEM photograph of palladium nanoclusters stabilized by 1,10-phenanthroline and oxygen and size distribution estimated from the photograph.

where d_0 is the nanocluster diameter in the starting solution, and n_i and n_m are the quantities of the ionic and metallic palladium respectively. In the present case $n_i = n_m$, so Eqn [2] leads to Eqn [3]:

$$d = \sqrt[3]{2d_0} \qquad (3)$$

The mean diameters of a series of Pd–PVP–Et (1/4) estimated from the TEM photographs are 2.53 nm, 3.03 nm, and 4.01 nm, whereas those calculated from Eqn [3] are 2.53 nm, 3.19 nm, and 4.02 nm respectively. The experimental results are in good agreement with the calculated ones. The original nanoclusters have a size distribution from 1.25 to 3.50 nm. Assuming that each nanocluster grows according to Eqn [3], the second and third nanoclusters are predicted to have a size distribution from 1.57 to 4.47 nm and from 1.98 to 5.56 nm respectively. Those results are also in good agreement with the experimental ones, indicating that the size distribution of the starting nanoclusters greatly influences that of the stepwise-synthesized nanoclusters.

Fig. 6 shows TEM photographs of Rh–TOAB, Pt–TOAB and Pd–TOAC nanoclusters and their size distributions estimated from the photographs. They are quite small in size and have rather narrow size distributions.

Table 2 Mean diameter, standard diviation, and crystal structure of the various noble-metal nanoclusters

Metal nanocluster	Mean diameter (nm)	Standard deviation (nm)	Crystal structure
Pd–PVP-Et(1/1)	2.88	0.745	Single crystal
Pd–DDAPS	3.20	0.975	Single crystal
Pd–phen	2.63	0.646	Single crystal
Pd–PVP-Pr(2/3)	2.19	0.493	Single crystal
Pd–PVP-Et(1/4)	2.53	0.400	Single crystal
Pd–PVP-Et(1/4)2	3.03	0.488	Single crystal + twin
Pd–PVP-Et(1/4)3	4.01	0.677	Single crystal + twin
Pd–TOAC	2.06	1.360	Single crystal
Pd/Pt–PVP	2.63	0.380	Single crystal
Pt–PVP	2.81	0.514	Single crystal
Pt–DDPAS	1.61	0.435	Single crystal
Pt–(DDPAS)p	2.86	0.578	Single crystal
Pt–TOAB	1.33	0.260	Single crystal
Rh–PVP	2.58	0.399	Single crystal
Rh–DDAPS	2.00	0.415	Single crystal
Rh–TOAB	1.44	0.388	Single crystal

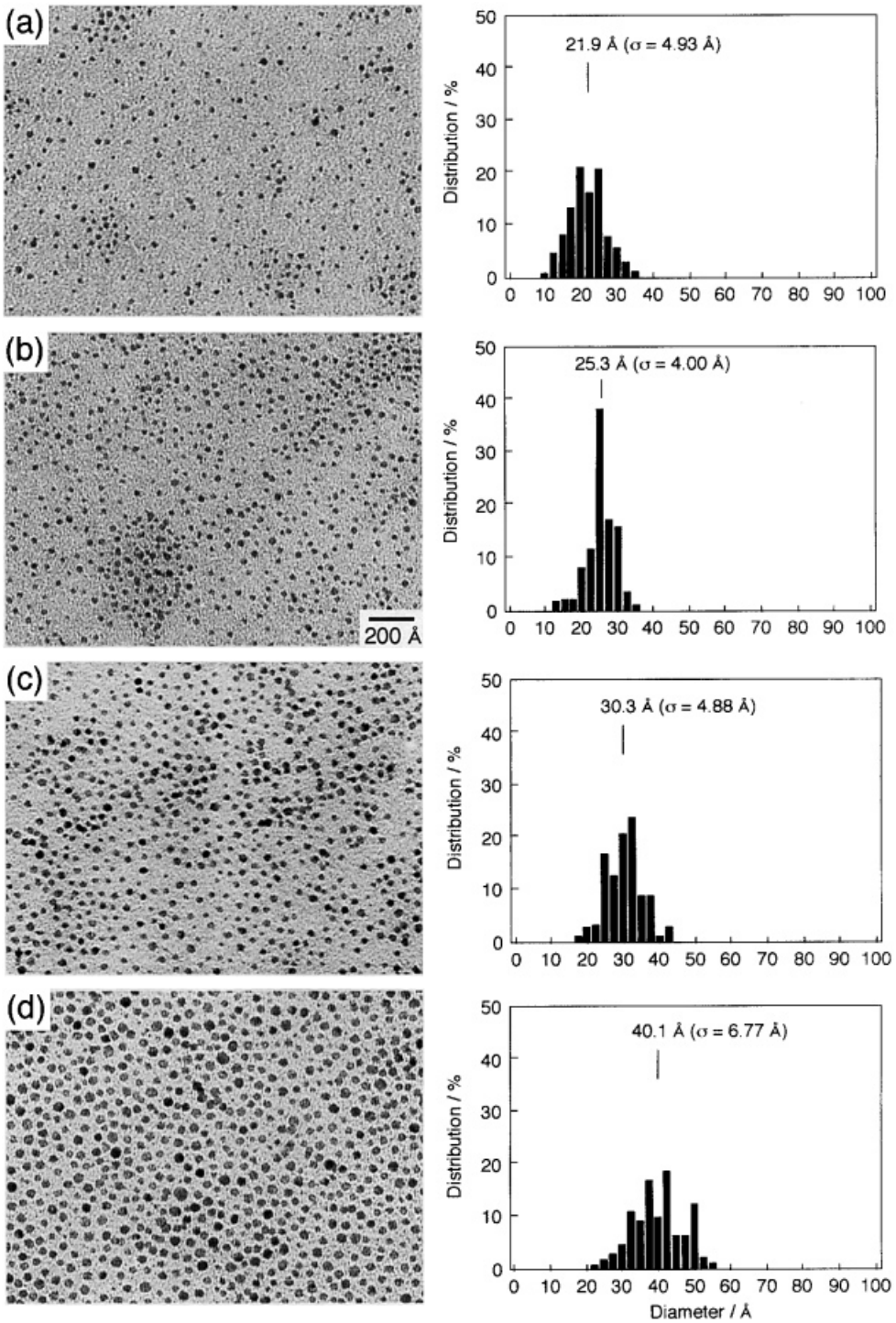

Figure 5 TEM photographs of Pd–PVP nanoclusters synthesized by a one-step and a stepwise growth reaction and their size distributions estimated from the photographs. (a) Pd–PVP–Pr(2/3), (b) Pd–PVP–Et(1/4), (c) Pd–PVP–Et(1/4)2, and (d) Pd–PVP–Et(1/4)3.

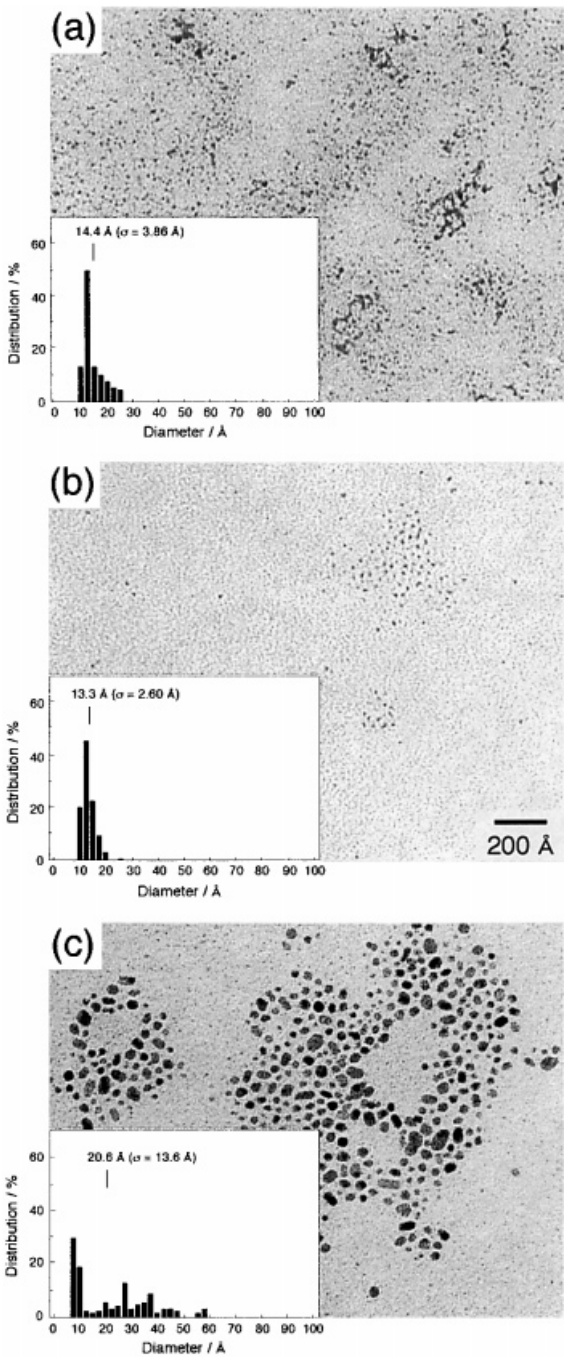

Figure 6 TEM photographs of (a) Rh–TOAB (b) Pt–TOAB and (c) Pd–TOAC nanoclusters and size distributions estimated from the photographs.

The mean diameters and standard deviations of the metal nanoparticles employed here are summarized in Table 2.

Crystal-structure of metal nanoclusters

The crystal structure of the metal nanoclusters employed in this study was investigated by HRTEM. Figures 7 to 10 present HRTEM images of metal nanoclusters, which correspond to the samples given in Figs 2 to 5 respectively, and Table 2 summarizes their crystal structures. In Fig. 7 all the metal–PVP nanoclusters show lattice images, and the lattice spacings of (111) planes, 0.23 nm, are in good agreement with those of bulk palladium, platinum and rhodium.[13] Therefore, the metal–PVP nanoclusters are single crystals and have fcc structures like to bulk metals. Similar results from the HRTEM observations apply to the metal nanoclusters protected by (DDAPS)p, DDAPS, or phen and oxygen. They are concluded to be single crystals and have fcc structures like to bulk metals (see Figs 8 and 9). Both the Pd–PVP–Pr(2/3) and Pd–PVP–Et(1/4) nanoclusters are also single crystals with fcc structures, whereas the Pd–PVP–Et(1/4)2 and Pd–PVP–Et(1/4)3 contain twinned particles, in which two single crystals with fcc structures combine with each other (see Fig. 10).

Diffusion coefficients and stokes radii

Metal nanoclusters stabilized by TOAB and TOAC

Platinum and rhodium nanoclusters stabilized by TOAB have small diameters (1.44 nm and 1.33 nm respectively) with quite narrow size distributions, as shown in Fig. 6. These nanoclusters can be dissolved to a clear solution in THF and toluene. THF solutions of 0.02% (wt/vol) M–TOAB (M = Rh or Pt) also containing 0%, 0.2%, and 3% (wt/vol) TOAB were injected into THF solutions containing 0%, 0.2% and 3% (wt/vol) TOAB respectively. In all cases the concentration profiles after diffusion dispersion (dispersion peaks) could be fit by Eqn [1] reasonably well, and two examples are shown in Fig. 11. The diffusion coefficients obtained are listed in Table 3, together with the solvent viscosities η, and the Stokes radius r_S, which were calculated using

$$r_S = k_B T/(6\pi\eta D) \qquad (4)$$

where k_B is the Boltzmann constant and T is the

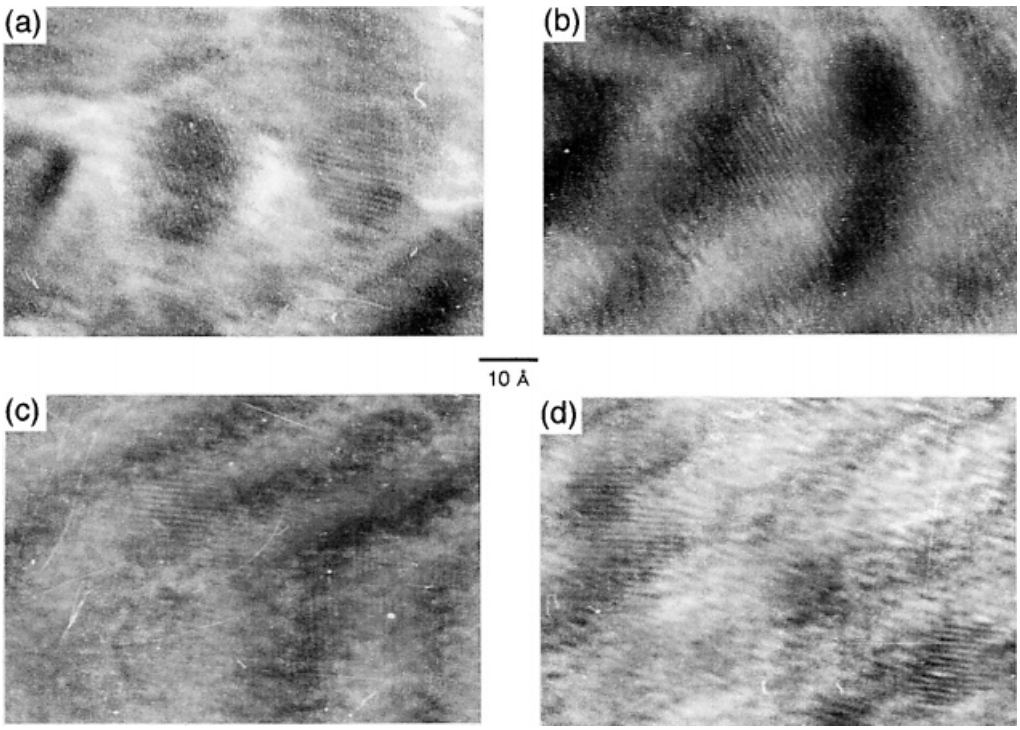

Figure 7 300 kV HRTEM images of (a) Pd–PVP–Et(1/1), (b) Pt–PVP, (c) Rh–PVP, and (d) Pd/Pt–PVP nanoclusters.

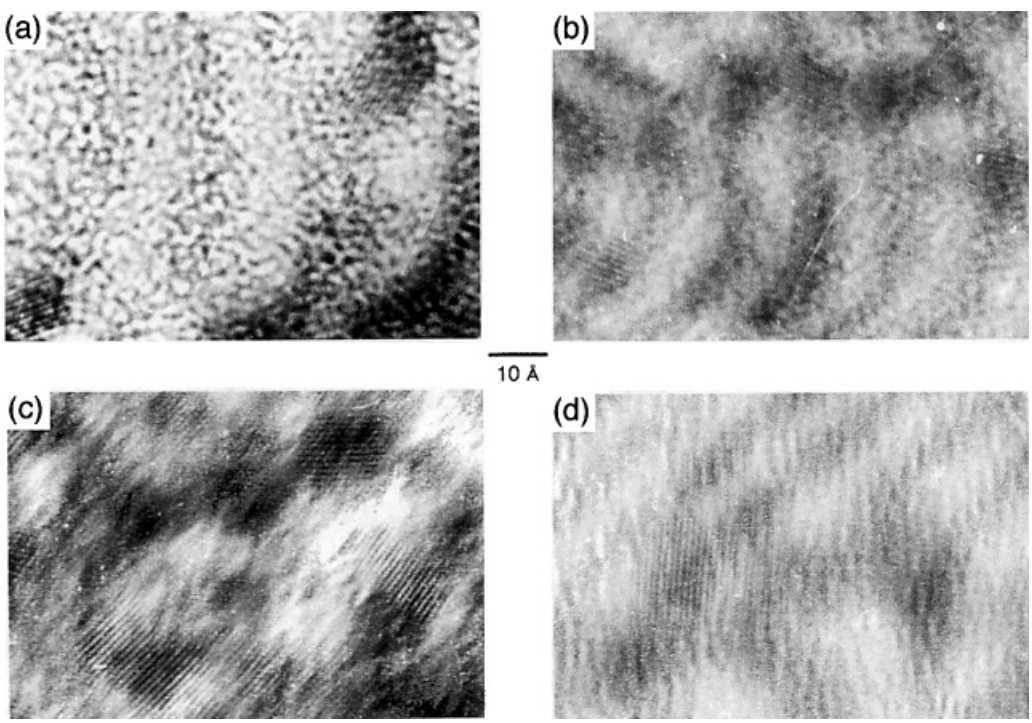

Figure 8 300 kV HRTEM images of (a) Pt–(DDAPS)p, (b) Pt–DDAPS, (c) Rh–DDAPS, and (d) Pd–DDAPS nanoclusters.

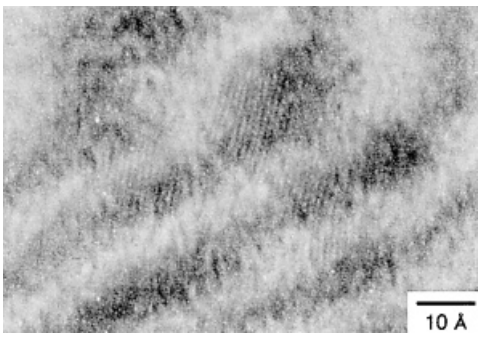

Figure 9 300 kV HRTEM images of palladium nanoclusters stabilized by 1,10-phenanthroline and oxygen.

absolute temperature. Stokes radii show no dependency on the TOAB concentration, either for Rh–TOAB or Pt–TOAB, which suggests that TOAB molecules are tightly bound to the metals and are not dissociating. In the case of Rh–TOAB, by subtracting the metal core radius ($d/2 = 0.67$ nm) from the Stokes radius ($r_S = 2.1$ nm), the thickness of the protective layer is calculated to be 1.4 nm. As is shown in Fig. 12, this thickness corresponds to the uni-molecular thickness of TOAB. In the case of Pt–TOAB, r_S (1.8 nm) and $d/2$ (0.72 nm) give the thickness of the protective layer to be 1.1 nm. Similar results have already been observed by our group for surfactant-stabilized metal nanoclusters.[12]

In the case of palladium nanoclusters protected by TOAC, when a solution was injected into THF, tailed dispersion peaks were obtained. The result may suggest that the protecting ability of TOA^+ is not so strong as in the rhodium and platinum cases. Figure 13 shows a dispersion peak when a Pd–TOAC solution was injected into THF containing 0.2% TOAB. As seen in Fig. 13a, the agreement between the observed and the fitted curves is poor when fit with Eqn [1]. When the peak is fit by a two-component equation

$$E(t) = (t_R/t)^{1/2} E_{max} \left[A_1 \exp\left\{ -12D_1 (t - t_R)^2 / r^2 t \right\} + A_2 \exp\left\{ -12D_2 (t - t_R)^2 / r^2 t \right\} \right] \quad (5)$$

the agreement between observed and fitted curves is good (Fig. 13b). The results were more or less similar to this when solutions were injected into

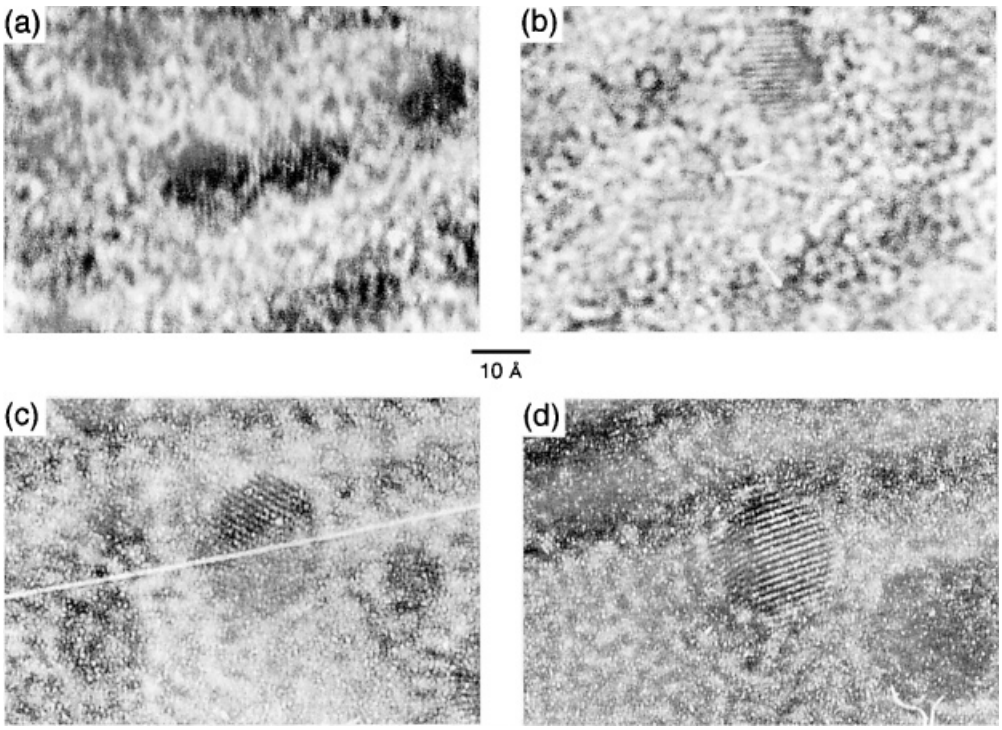

Figure 10 300 kV HRTEM images of (a) Pd–PVP–Pr(2/3), (b) Pd–PVP–Et(1/4), (c) Pd–PVP–Et(1/4)2, and (d) Pd–PVP–Et(1/4)3 nanoclusters.

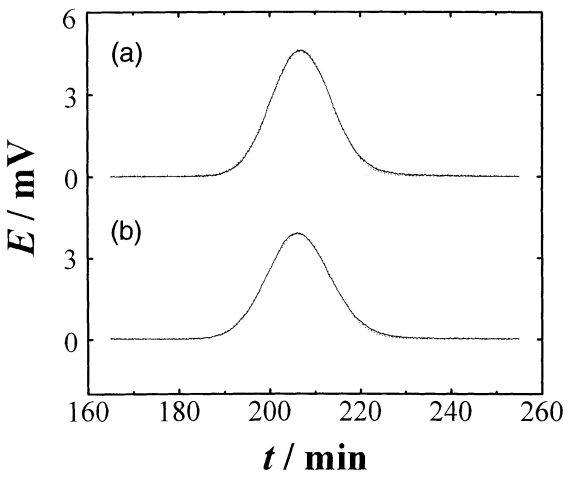

Figure 11 Dispersion peaks for Rh–TOAB in THF at 298.15 K. (a) 0.02% (wt/vol) Rh–TOAB solution was injected into THF. (b) 0.02% (wt/vol) Rh–TOAB solution also containing 3% (wt/vol) TOAB was injected into 3% (wt/vol) TOAB solution.

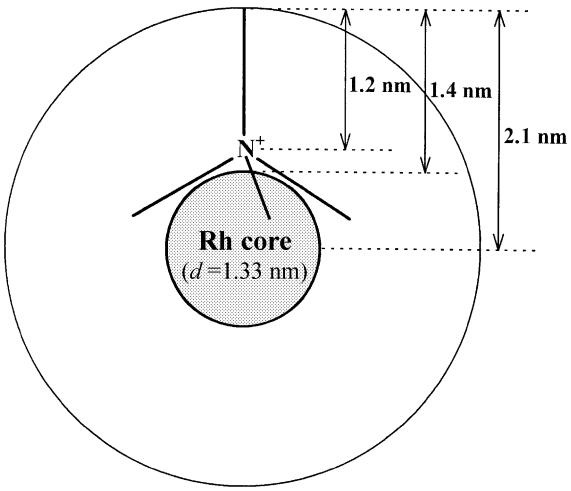

Figure 12 Model of the metal core and the protective layer.

THF containing 1.0% TOAB. The D_1 and D_2 values and the corresponding Stokes radii are listed in Table 3.

Stokes radii, 0.92 and 1.02 nm, calculated from faster components of the diffusion coefficients are smaller than the size of TOA^+ ion. The TEM photograph for Pd–TOAC (Fig. 6) shows the existence of particles of 0.4 (29 %) and 0.5 nm (18.5 %) diameter. When these small particles are protected by TOA^+ ions, it is likely that there are vacant spaces between the TOA^+ ions. This may be the reason for the smaller Stokes radius than the molecular size of the TOA^+ ion. Stokes radii, 6.0 and 5.0 nm, calculated from the slower component of the diffusion coefficients are larger than the sum of the metal cluster radius and the size of the TOA^+ ion (2.1 nm as maximum, see Fig. 12). The results may suggest that there are some aggregated particles.

Metal nanoclusters stabilized by PVP

In order to measure the diffusion coefficients, the ethanol solutions of PVP-stabilized metal nanoclusters were prepared at least twice independently, and more than four dispersion peaks were obtained

Table 3 Diffusion coefficients and Stokes radii for Rh–TOAB, Pt–TOAB and Pd–TOAC in THF solution at 298.2 K

Solution[a]	Solvent	η/cP	$D/10^{-10}$ m^2 s^{-1}	r_S/nm
Rh–TOAB	THF	0.463	2.26[b]	2.09
Rh–TOAB	0.20% (wt/vol) TOAB in THF	0.464	2.23[c]	2.11
Rh–TOAB	3.0% (wt/vol) TOAB in THF	0.525	1.96 ± 0.02	2.13 ± 0.02
Pt–TOAB	THF	0.463	2.53 ± 0.13	1.87 ± 0.10
Pt–TOAB	0.20% (wt/vol) TOAB in THF	0.464	2.81[d]	1.70
Pt–TOAB	3.0% (wt/vol) TOAB in THF	0.525	2.22 ± 0.10	1.88 ± 0.08
Pd–TOAC	0.20% (wt/vol) TOAB in THF	0.464	5.11 ± 0.21[e]	0.92 ± 0.04
			0.80 ± 0.08[e]	5.95 ± 0.57
Pd–TOAC	1.0% (wt/vol) TOAB in THF	0.483	4.44 ± 0.15[e]	1.02 ± 0.03
			0.90 ± 0.03[e]	5.04 ± 0.17

[a] The solutions contained 0.02% (wt/vol) colloids and the same concentration of TOAB or TOAC as respective solvents.
[b] Average value of 2.21, 2.29, and 2.27.
[c] Average value of 2.25, 2.25, and 2.20.
[d] Average value of 2.79 and 2.83.
[e] These values are D_1 and D_2 values obtained using Eqn. [5].

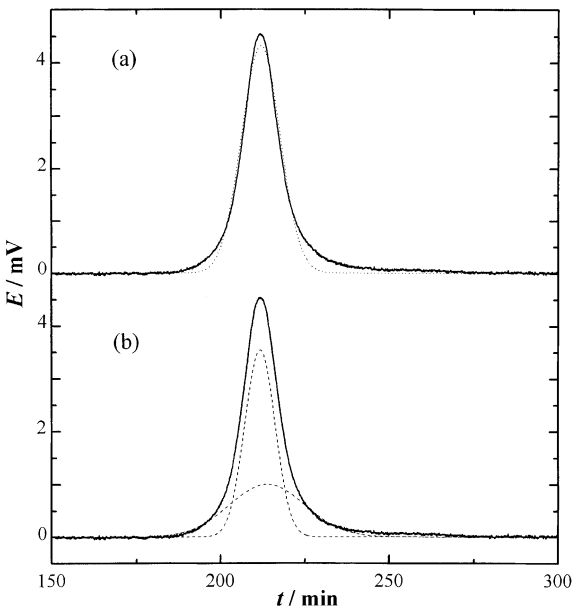

Figure 13 Dispersion peak for Pd–TOAC in THF containing 0.2% (wt/vol) TOAB. Solid lines show the observed curve, dotted lines show the fitted curves by (a) a single-component Gaussian function (Eqn [1]) and (b) two-component Gaussian function (Eqn [4]), and two dashed lines show two calculated contributions of each component.

altogether for each metal nanocluster. The agreements between observed and fit curves using Eqn [1] were reasonably good for Pd–PVP–Pr(2/3), Pd–PVP–Et(1/4), Pd–PVP–Et(1/4)2, and Pd–PVP–Et(1/4)3. An example is shown in Fig. 14 for Pd–PVP–Pr(2/3). Diffusion coefficients calculated using Eqn [1] are listed in Table 4 together with

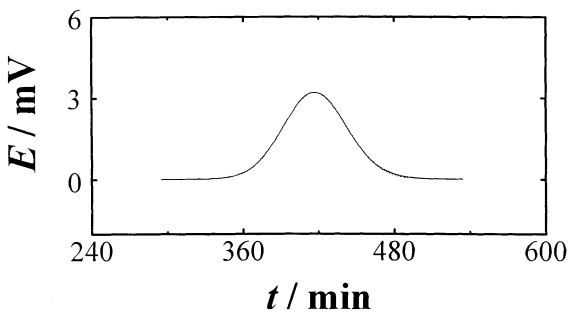

Figure 14 Dispersion peak for Pd–PVP–Pr(2/3) in ethanol. Solid line shows the observed curve and dotted line shows the fit curve by a single-component Gaussian function (Eqn [1]).

Table 4 Diffusion coefficients and Stokes radii of PVP-stabilized metal nanoclusters in ethanol at 298.2 K

Metal nanocluster	$D/10^{-11}$ m^2 s^{-1}	r_S/nm
Pd–PVP–Pr(2/3)	3.12 ± 0.18	6.48 ± 0.39
Pd–PVP–Et(1/4)	3.25 ± 0.25	6.24 ± 0.48
Pd–PVP–Et(1/4)2	2.95 ± 0.03	6.84 ± 0.07
Pd–PVP–Et(1/4)3	2.56 ± 0.02	7.88 ± 0.06
Pd/Pt(4/1)–PVP	2.85 ± 0.10	7.09 ± 0.26
	4.23 ± 0.18[a]	4.77 ± 0.20[a]
	1.15 ± 0.16[a]	17.8 ± 2.6[a]

[a] These are D_1 and D_2 values obtained using Eqn [5] and the corresponding r_S values.

standard deviations. The D values are one order of magnitude smaller than those for the rhodium and platinum nanoclusters protected by TOAB in THF. Dispersion peak for Pd/Pt–PVP is shown in Fig. 15. In this case, when fit with Eqn [1], the agreement between observed and fit curves was poor (Fig. 15a). The D_1 and D_2 values are also listed in Table 4 for this system.

Also listed in Table 4 are Stokes radii, which were calculated using the viscosity of ethanol (1.083 cP). Comparison of the r_S values in Table 4 with radii obtained by TEM shows that the thickness of the protective layer is surprisingly large, i.e. 5–6 nm for the five nanoclusters using D

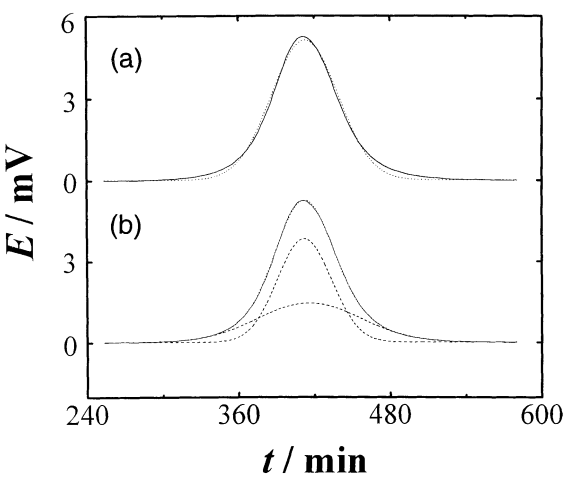

Figure 15 Dispersion peak for Pd/Pt–PVP in ethanol. Solid lines show the observed curve, dotted lines show the fit curves by (a) a single-component Gaussian function (Eqn [1]) and (b) two-component Gaussian function (Eqn [4]), and the dashed lined shows the calculated contributions of each component.

values obtained using Eqn [1], and 3.5 nm for the Pd/Pt–PVP nanocluster using the D_1 value obtained from Eqn [5]. The D_2 value for the Pd/Pt–PVP nanocluster gives an astonishingly large r_S value (18 nm). This may mean that there are some aggregated particles in solution.

Dispersion peaks for Pt–PVP could not be fit by neither Eqn [1] or Eqn [5]. Although the peaks for Rh–PVP could be fit by Eqn [1], r_S values were as large as 28 nm. The TEM photograph for this dispersion (Fig. 2c) shows aggregated particles. Although some particle aggregation may have happened in the process of the sample preparation for the TEM observation, dispersion peaks suggest that there are aggregated particles in solution.

These kinds of aggregation of PVP-protected metal nanoclusters in colloidal dispersions were also observed by small-angle X-ray scattering analysis of colloidal dispersions of PVP-stabilized platinum, rhodium, and Pt/Rh nanoclusters.[14] The authors have proposed a hierarchy in spatial organization of metal nanoclusters. The hierarchy starts from the smallest 'fundamental metal nanoclusters', 'superstructure of fundamental metal nanoclusters', and then finally 'higher-order organization of superstructures'. The large layer size observed in the present experiments could suggest the superstructure is composed of polymer and metal nanoclusters.

Metal nanoclusters stabilized by DDAPS

Dispersion peaks for Pt–DDAPS, Pd–DDAPS, and Rh–DDAPS could not be fit by Eqn [1]. When these peaks were fit by Eqn [5], one component gave r_S values of 5–9 nm and the other component gave even larger r_S values. TEM photographs for these colloids (Fig. 3) again show aggregated particles.

Catalytic activity in homogeneous systems

The catalytic activities of ligand-stabilized metal nanoclusters were evaluated for hydrogenation of COD and MA in homogeneous systems. The results are summarized in Table 5 along with mean diameters and standard deviations of the nanoclusters. The Pd/Pt–PVP nanoclusters show the highest catalytic activity for hydrogenation of COD and MA. It is consistent with our previous study,[15] in which bimetallic nanoclusters are more active and selective catalyst than the corresponding monometallic nanoclusters. We have reported that the Pd/Pt (4:1 in mole ratio) nanoclusters stabilized by PVP (40.1 times the total amount of metal ions in moles) have a relatively high activity for selective partial hydrogenation, although palladium nanoclusters are relatively active but platinum nanoclusters inactive as a catalyst for the partial hydrogenation of COD. In the present study, the Pd/Pt nanoclusters stabilized by PVP (once the total amount of metal ions in moles) also show higher catalytic activity than the corresponding monometallic nanoclusters.

Table 5 demonstrates that monometallic nanoclusters in any form are more active than the commercial metal-black catalysts, in which considerable aggregation of large particles was observed. In a series of palladium and rhodium

Table 5 Catalytic activity for hydrogenation of COD and MA[a]

Metal nanocluster	d/nm	σ/nm	r_{H_2}/ mol-H_2 mol-M^{-1} s^{-1}	
			COD	MA
Pd–PVP	2.88	0.745	3.35	2.48
Pd–DDAPS	3.20	0.970	3.29	2.41
Pd–phen	2.63	0.646	1.59	1.01
Pd–black	—	—	0.0057	0.0045
Pd/Pt–PVP	2.63	0.380	4.70	4.77
Pt–PVP	2.81	0.514	0.30	0.45
Pt–DDAPS	1.61	0.435	0.41	0.53
Pt–(DDAPS)p	2.86	0.578	0.32	0.25
Pt–black	—	—	0.0053	0.0042
Rh–PVP	2.58	0.399	1.53	3.30
Rh–DDAPS	2.00	0.415	1.43	2.44
Rh–black	—	—	0.0056	0.0048

[a] Conditions: [substrate] = 25 mmol dm^{-3}; [catalyst] = 0.01 mmol dm^{-3}; solvent, ethanol at 30 °C.

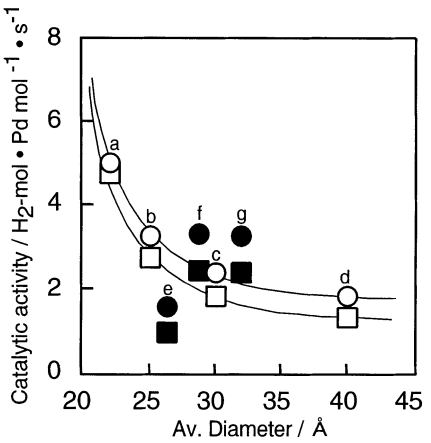

Figure 16 Plot of catalytic activity for the hydrogenation of COD (○) and MA (□) *vs* the average diameter of palladium nanoclusters. (a) Pd–PVP–Pr(2/3), (b) Pd–PVP–Et(1/4), (c) Pd–PVP–Et(1/4)2, (d) Pd–PVP–Et(1/4)3, (e) Pd–phen, (f) Pd–PVP–Et(1/1) and (g) Pd–DDAPS.

nanoclusters, the PVP-stabilized nanoclusters are more active than the DDAPS- or phen-stabilized ones. However, Pt–DDAPS nanoclusters have higher catalytic activity than Pt–PVP. The high catalytic activity of Pt–DDAPS nanoclusters may be due to their small particle size. In the case of rhodium nanoclusters, Rh–DDAPS nanoclusters are a little smaller in average diameter but less active as catalysts for hydrogenation of COD and MA than Rh–PVP nanoclusters. This may be due to the possible aggregation and wider dispersion in Rh–DDAPS than Rh–PVP nanoclusters.

In order to examine the effect of the particle size of catalysts, palladium nanoclusters with the different particle size, i.e. Pd–PVP–Pr(2/3), Pd–PVP–Et(1/4), Pd–PVP–Et(1/4)2, and Pd–PVP–Et(1/4)3 were prepared by a stepwise growth method as described above. The palladium nanoclusters obtained in this manner were also submitted to measurement of the catalytic activity for hydrogenation. The results are plotted in Fig. 16 along with other data. The catalytic activity for hydrogenation of COD (○) gradually increases with decreasing particle size of the palladium nanocluster, and reaches a maximum (5.05 mol-H_2 mol-Pd^{-1} s^{-1}) when the average particle size is 2.2 nm. A similar relation is observed in hydrogenation of MA (□). However, the Pd–phen nanoclusters have a lower catalytic activity than that expected from the particle size. This is probably because the substrate, COD and MA, may not easily approach to active sites on the surface of Pd–phen nanoclusters, since phen molecules coordinate strongly to the metal, and cover the surface of palladium particles. A similar effect of strongly coordinating ligands has been observed for triphenylphosphine-stabilized platinum nanoclusters.[16]

Table 6 Dependence of catalytic activity of platinum nanoclusters for hydrogenation of MA upon the solvent[a]

	r_{H_2}/ mol-H_2 mol-Pt^{-1} s^{-1}	
Metal nanocluster	Water	Ethanol
Pt–PVP	0.36	0.45
Pt–DDAPS	0.45	0.53
Pt–(DDAPS)p	0.31	0.25

[a] Conditions: [substrate] = 25 mmol dm^{-3}; [catalyst] = 0.01 mmol dm^{-3}; at 30 °C. Solvent: water (30 ml) and ethanol (30 ml).

In order to examine the matrix effect of ligands, the catalytic activity of metal nanoclusters in water was compared with that in ethanol. The results are shown in Table 6. In the case of Pt–PVP and Pt–DDAPS nanoclusters, the activities in water are smaller than those in ethanol. The higher catalytic activity in ethanol than in water may be associated with the dispersibility of Pt–PVP and Pt–DDAPS in solution. In contrast, Pt–(DDAPS)p in ethanol, in which considerable aggregation was observed, has a lower catalytic activity than that in water.

Activity of the charcoal-supported palladium nanocluster catalysts

Because of the opportunity for comparison, all the metal nanoclusters were deposited on the same charcoal support to produce heterogeneous catalysts. The Pd–DDAPS on C catalyst has a metal content of 4.83 wt% palladium. The Pd–phen on C catalyst and the Pd–PVP on C catalyst both have a palladium content of 5 wt%.

Every catalyst was tested for four times in the hydrogenation of cinnamic acid, a standard substrate that is routinely applied for commercial industrial palladium catalysts. The set-up used for determining the catalyst activity is described elsewhere[8] and analogously built up to an industrial testing apparatus used for catalyst quality control. The highest activity of the catalysts is always found at the start of the reaction and, therefore, the hydrogen consumption in the first 5 min after catalyst activation (1 min) is taken as the measure for the maximal activity r_{H2}. This activity r_{H2} has

Table 7 Catalytic activity of charcoal-supported palladium nanoclusters

Catalyst	r_{H_2}/ mol-H_2 mol-Pd^{-1} s^{-1}
Pd–DDAPS on C	2.52 ± 0.057
Pd–phen on C	0.198 ± 0.019
Pd–PVP on C	0.0431 ± 0.0033

been measured as the uptake of hydrogen in moles per mole of palladium per second ($[r_{H2}]$ = mol-H_2 mol-Pd^{-1} s^{-1}).[8] Results are shown in Table 7.

For testing the stability of the apparatus during the test phase and for the determination of the standard deviation of the results, we have examined an industrial catalyst before, between and after the tests of the other catalysts. It was found that there was no trend in the measured values, which means that the reactor was in order during the test phase. The standard deviation of the mean values is about 7%. The maximal activities determined for the charcoal-supported palladium nanoclusters are in the ratio Pd–DDAPS on C catalyst:Pd–phen on C catalyst:Pd–PVP on C catalyst = 58.5:4.6:1. This means that in the cinnamic acid test the Pd–DDAPS on C catalyst is about 12 times more active than the Pd–phen on C catalyst and about 60 times more active than the Pd–PVP on C catalyst. This result is in strong contrast to the results for the hydrogenation of COD and MA in the homogeneous phase, where the PVP-stabilized palladium nanoclusters are the most active ones. We do not know the clear reason, but a possible explanation is due to the difference in aggregation structure of palladium nanoclusters on charcoal, since PVP might flocculate in the THF used for supporting the palladium nanoclusters. Further investigation will be necessary to prove the precise reason.

CONCLUSION

Comparison of characteristic properties, such as particle size and catalysis, was carried out for various ligand-stabilized noble-metal nanoclusters prepared by various chemical methods. The TEM observations show mean diameters and standard deviations of these metal nanoclusters (Table 2) that range from 1.3 to 4.0 nm and from 0.26 to 0.97 nm respectively, depending on the kind of metal and the preparation method. If the relative standard deviations are calculated for these nanoclusters examined in the present investigation, the smallest value (14%) is obtained for Pd/Pt–PVP, i.e. the Pd/Pt bimetallic nanoclusters prepared by alcohol reduction in the presence of PVP. Among monometallic nanoclusters, Pd–PVP–Et(1/4) (16%), Pt–PVP (18%), and Rh–PVP (16%) have the smallest relative standard deviations for palladium, platinum and rhodium nanoclusters respectively. These results suggest that PVP is the best stabilizer, even though only a small amount (PVP/M = 1) of PVP was used.

A Taylor dispersion method was applied to the present colloidal dispersion system in order to understand the thickness of the protective layer. This is successful for the surfactant-stabilized metal nanoclusters like Rh–TOAB, Pt–TOAB and Pd–TOAC (Table 3). However, very large values were obtained for the PVP-stabilized metal nanoclusters. This is probably because the adsorbed PVP molecules could expand into the ethanol solvent and sometimes form aggregated superstructures. In this case, not only one, but also two or three components can be obtained (Table 4), suggesting a hierarchy in spatial organization of polymer-stabilized metal nanoclusters in dispersions.

Catalytic activities of noble-metal nanoclusters are much higher than the corresponding commercial metal-black catalysts. Among palladium, platinum and rhodium nanoclusters, the catalytic activity for hydrogenation of olefin increases in the following order, depending on the kind of metal: Pt < Rh < Pd. The Pd/Pt bimetallic nanocluster shows higher activity than palladium nanoclusters. As for palladium nanoclusters, the activity depends on the particle size, i.e. the smaller the size, the higher the activity in general. However, the particle size is not the only parameter to determine the activity. The stabilizer could influence the activity (see Fig. 16). For example, 1,4-phenanthroline is a good stabilizer to stabilize particles, but a bad stabilizer for catalysis. In addition, it should be mentioned that the present catalytic activities were measured by the catalytic reaction in the dispersed solution. The results would be quite different if the catalytic activities were measured by the supported catalyst using the same nanoclusters.

Acknowledgements The financial supports of the Japan Society for the Promotion of Science (JSPS) and Deutsche Forschungsgemeinschaft (DFG) are gratefully acknowledged.

REFERENCES

1. Schmid G. (ed). *Clusters and Colloids*, VCH: Weinhiem, 1994.
2. (a) Schmid G. *Chem. Rev.* 1992; **92**: 1709. (b) Hirai H, Chawanya H, Toshima N. *Reactive Polym*. 1985; **3**: 127.
3. Bradley JS. In *Clusters and Colloids*, Schmid G (ed.). VCH: Weinheim, 1994; chapter 6.
4. (a) Bönnemann H, Brijoux W. In *Advanced Catalysts and Nanostructured Materials*, Moser W (ed.). Academic Press: New York, 1996; chapter 7. (b) Bönnemann H, Braun G, Brijoux W, Brinkmann R, Schulze Tilling A, Seevogel K, Siepen K. *J. Organomet. Chem.* 1996; **520**: 143. (c) Bönnemann H, Brijoux W, Siepen K, Hormes J, Franke R, Pollmann J, Rothe J. *Appl. Organomet. Chem.* 1997; **11**: 783.
5. (a) Hirai H, Toshima N. In *Tailored Metal Catalysts* Iwasawa Y. (ed.). D. Reidel: Dordrecht, 1986; 87. (b) Hirai H, Toshima N. In *Polymeric Materials Encyclopedia*. vol. 2/c, Salamone JC. (ed.). CRC Press: Boca Raton, 1996; 1310. (c) Toshima N. In *Fine Particles Science and Technology — From Micro to Nanoparticles*, Pelizzetti E. (ed.). Kluwer Academic: Dordrecht, 1996; 371. (d) Toshima N, Yonezawa T. *New J. Chem.* 1998; **22**: 1179.
6. (a) Hirai H, Nakao Y, Toshima N. *J. Macromol. Sci. Chem. A* 1978; **12**: 1117. (b) Toshima N. *Macromol. Symp.* 1996; **105**: 111.
7. Teranishi T, Miyake M. *Chem. Mater.* 1998; **10**: 594.
8. (a) Bönnemann H, Brijoux W, Brinkmann R, Fretzen R, Joussen T, Köppler R, Korall B, Neiteler P, Richter J. *J. Mol. Catal.* 1994; **86**: 129. (b) Bönnemann H, Brinkmann R, Köppler R, Neiteler P, Richter J. *Adv. Mater.* 1992; **4**: 804.
9. Schmid G, Harms M, Malm JO, Bovin JO, Ruitenbeck J, Zandbergen HW, Fu WT. *J. Am. Chem. Soc.* 1993; **115**: 2046.
10. Taylor GI. *Proc. R. Soc. London Ser. A* 1953; **219**: 186. 1954; **225**: 473.
11. Alizadeh A, Nieto de Castro CA, Wakeham WA. *Int. J. Thermophys.* 1980; **1**: 243. Turrell HJV, Harrism KR. *Diffusion in Liquids. A Theoretical and Experimental Study*. Butterworths: London, 1984; 193.
12. (a) Yonezawa T, Tominaga T, Toshima N. *Langmuir* 1995; **11**: 4601. (b) Tominaga T, Nishinaka M. *J. Chem. Soc. Faraday Trans.* 1993; **89**: 3459.
13. JCPDS–ICDD, PDF-2 Data Base.
14. Hashimoto T, Saijo K, Harada M, Toshima N. *J. Chem. Phys.* 1998; **109**(13): 5627.
15. (a) Toshima N, Kushihashi K, Yonezawa T, Hirai H. *Chem. Lett.* 1989; 1976. (b) Toshima N, Yonezawa T, Kushihashi K. *J. Chem. Soc. Faraday Trans.* 1993; **89**: 2537.
16. Toshima N, Nakata K, Kitoh H. *Inorg. Chim. Acta* 1997; **265**: 149.

